IEEE Access
Multidisciplinary | Rapid Review | Open Access Journal

Received March 3, 2021, accepted April 3, 2021, date of publication April 12, 2021, date of current version April 20, 2021.

Digital Object Identifier 10.1109/ACCESS.2021.3072662

Data-Driven Laser Plane Optimization for High-Precision Numerical Calibration of Line Structured Light Sensors

JINGBO ZHOU[1], LAISHENG PAN[1], YUEHUA LI[1], RENJIE DU[2], AND FUXIANG ZHANG[1]
[1]School of Mechanical Engineering, Hebei University of Science and Technology, Shijiazhuang 150018, China
[2]Hebei Boxline Intelligent Equipment Technology Company Ltd., Handan 057150, China

Corresponding author: Yuehua Li (yuehua.hrbin@163.com)

This work was supported in part by the National Natural Science Foundation of China under Grant 51705130, in part by the S&T Program of Hebei under Grant 20311804D, and in part by the Natural Science Foundation of Hebei Province under Grant E2016208084.

ABSTRACT Line structured light sensor has been applied in various three dimensional (3D) measurement scenes with the advantages of non-contact, low cost and high speed. Its accuracy, which is directly determined by the calibration method, needs to be further improved to fulfill the measuring tasks of precision parts. Here, we proposed a numerical method that can eliminate the errors of the model based methods through two strategies. One is the establishment of the numerical mapping relationship between stripe pixel coordinates and their world coordinates through piecewise cubic interpolation. Corner points of a checkerboard target are used to obtain sufficient interpolating nodes. This target can be manually aligned with the laser plane and the alignment error would be eliminated via the point projection. The other is the data-driven laser plane optimization. The data set of reference interval distance is computed based on the invariance of cross ratio. The optimization model is to minimize the root mean squared error of measured interval distances by adjusting the laser plane coefficients. After the optimization, a higher numerical mapping relationship can be achieved. It bypasses the camera and the distortion models and reaches a calibration error of only 0.005mm. The comparison studies and the measurement of the steps further validate the proposed method.

INDEX TERMS Accuracy analysis, calibration, direct coordinate mapping, laser plane optimization, line structured light sensor, machine vision.

I. INTRODUCTION

Line structured light sensor (LSLS) has the advantages of non-contact, simple construction, high speed, moderate accuracy and low cost [1]. It now gains more and more applications in railway inspection [2], geometrical measurement [3], [4], quality evaluation Lu *et al.* [5], Based on the laser triangulation principle, the profile under inspection is usually computed via the perturbed stripe image and the pre-calibrated sensor parameters like the intrinsic parameters and the laser plane. The calibration method, that directly determines the measuring accuracy, is a key issue for the research and the application of LSLS.

In early method, thin strained threads were used to get bright light dots by intersecting with the laser plane [6]. To obtain world coordinates of the dots, auxiliary measuring device is needed and the coordinate accuracy is hard to be guaranteed. Another method is to obtain the feature points with a zigzag [7]. Like the thin strained threads method, the calibration accuracy is also restricted by the limited feature points. Huynh *et al.* [8] presented a calibration method by use of a non-coplanar target. The image to world transformation matrix is computed based on the invariance of cross ratio. Zhou and Zhang [9] presented a complete calibration method by use of a freely moved planar target. This method is easy applicable and suited for on-site calibration, but few feature points can be obtained for fitting of laser plane. Wei *et al.* [10] obtains more points on light plane via the invariance of double cross ratio. This method simplified the calibration at the expense of fabricating an elaborated 3D target.

For the camera calibration methods are increasingly mature [11], current researches generally focus on the calibration of laser plane. The representative methods can be based

The associate editor coordinating the review of this manuscript and approving it for publication was Wei Liu.

on the collinear condition of three planes [12], the double virtual circles [13], the 3D calibration target and a height gauge [14], the vanish points [15], the concentric circle [16], the standard ceramic ball [17], the parallel moving target [18], the front coating plane mirror [19], etc. Beside these, Santolaria *et al.* [20] presents a one-step calibration procedure for the sensor calibration and the integration with the coordinate measuring machine by use of specifically designed gauge objection. Xie and Zhang [21] integrated the sensor with two linear stages where the laser plane and the translation matrix between the sensor and the motion coordinate system were calibrated simultaneously. Zhou *et al.* [22] proposed a calibration method by use of a reference target where the laser plane is also computed based on the intrinsic parameters. Pan and Liu [23] improved the accuracy of laser plane equation by correcting image deviation. Based on the articular arm, they also developed a global calibration method of multi-vision sensors which is suitable for on-site complex environment [24]. Generally, all the methods above rely on the camera and the laser plane models. Thus, the models and their calibration errors would affect the measuring results directly.

Sensor accuracy is one of the most concerned issues for the calibration and the application [25]. Current calibration error generally ranges from hundreds to tens of microns, and seems to have reached their limits [26]. With the increasing demands for geometrical measurement of precision parts, higher accuracy is required. Besides the laser plane, camera distortion also plays a key role. The traditional distortion models including the radial distortion [27], the rational radial distortion [28], the radial and tangential distortion [29], and the radial, tangential and thin prism distortions [30]. Many other new models are also proposed for better distortion correction [31, 32]. To achieve a higher accuracy, more distortion forms need to be taken into consideration. The models are also getting more and more complicated together with their solution process. However, the distortion is determined by the manufacture and the assemble quality of the lens which is of uncertainty between each other. Noticed the complexity of the distortions, Yang *et al.* [33] proposed a hybrid calibration method to correct the distortions using a back-propagation network. This method improves the precision effectively, but needs auxiliary parts to get training samples. The problems of the network like over fitting and poor generalization also need to be treated carefully. Therefore, it is quite difficult to remove the effects of the distortions on the measurement results of LSLS [34].

It is clear that a homographic mapping relationship exists between the points on laser plane and image plane. So is it possible to establish a numerical mapping relationship that can eliminate all the model errors? Li *et al.* [35] established the mapping relationship via carefully aligning the target surface with the laser plane. The laser plane is physically untouched. Just by evaluating the stripe on the target surface visually, the alignment accuracy is hard to be guaranteed. Zou *et al.* [36] fixed standard gauge blocks onto a precision linear stage and established the mapping relationship between the edge features and their world coordinates. The parallel requirement between the 2D motion and the laser plane is hard to be achieved. Moreover, the extraction accuracy of the feature points is deteriorated by the reflections at the corner and then restricts the calibration accuracy. Therefore, the greatest challenge is to get sufficient points on laser plane with high accurate coordinates.

In this paper, a numerical mapping relationship between stripe pixel coordinates and their world coordinates is established. It not only takes into account the misalignment between the target and the laser plane, but also involves a data-driven optimization of the laser plane. The calibration results are discrete mapping points and can bypass the inaccuracy of the distortion model and the laser plane equation. Detail procedures are presented as follows.

II. CALIBRATION PRINCIPLE

Measuring principle of LSLS is illustrated by Fig. 1, where $O_wX_wY_wZ_w$ is the world coordinate frame (WCF), $o_cx_cy_cz_c$ is the camera coordinate frame (CCF), ouv is the image coordinate frame (ICF) with $ou//o_cx_c$ and $ov//o_cy_c$, and f is the focal length. The laser plane Π_L, which emits from the laser projector, intersects the object under inspection. The diffused stripe from the object is projected on the image plane Π_I and captured by the matrix CCD camera. Based on the pinhole model, an arbitrary point $P(X, Y, Z)$ in WCF has one unique projection point $C(u, v)$ on Π_I. P and C can be called a homographic mapping point pair. If plenty of mapping point pairs can be obtained, the world coordinates for an image points can be computed via interpolation. This strategy does not rely on the models of camera, lens distortion and laser plane.

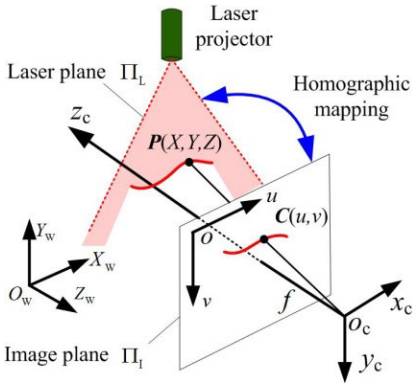

FIGURE 1. Measuring principle.

An intuitive method to get the mapping point pairs is to align the target surface Π_T with Π_L [35]. However, the alignment accuracy is hard to be guaranteed due to the untouchable nature of Π_L. To solve this problem, the point projection strategy is adopted, as shown by Fig. 2(a). In this figure, a high precision checkerboard target, also called the reference target, is manually aligned with the laser plane firstly. Then,

the coefficients of Π_L are calculated by use of the model based method in section 3.2. The kth corner point of the reference target P_k^T can be projected onto Π_L as P_k^L. The WCF is established with the left bottom point O_w as its origin. The $X_wO_wY_w$ plane is coincided with Π_L. Thus, the world coordinates of each projection point are the signed distances to the corresponding axis.

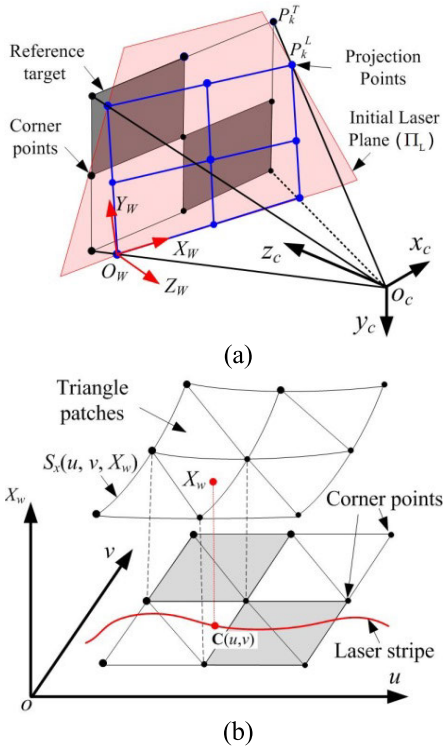

FIGURE 2. Calibration principle. (a) Projection of corner points onto initial laser plane, (b) Computation of world coordinates using cubic interpolation.

When pixel coordinates of each corner point are extracted from the target image, two mapping surfaces, named S_x and S_y, can be generated, respectively. Take S_x as example, it consists of many triangle patches by Delaunay triangulation of the corner points on Π_I, as shown by Fig. 2(b). For an arbitrary point $C(u, v)$ on stripe center line, its X_w value can be obtained via the cubic interpolation of the corresponding triangle patch. It is the same for the computation of Y_w. Therefore, it is a numerical method.

To remove the calibration error of Π_L, its coefficients are further optimized based on the root mean squared (RMS) error of measuring result. The completed flow chart of calibration procedures is show by Fig. 3. The reference interval distances are from a ceramic target with different poses and computed based on the invariance of cross ratio. The reference results do not rely the camera model and are widely accepted for the accuracy evaluation of the sensors [9], [15]–[17], [19], [20], [22], [23]. Together with the cubic interpolation process for measured distance calculation, the models are no more needed after the iterative loop of the optimization. Hence, the model errors can be generally eliminated and higher calibration accuracy can be expected.

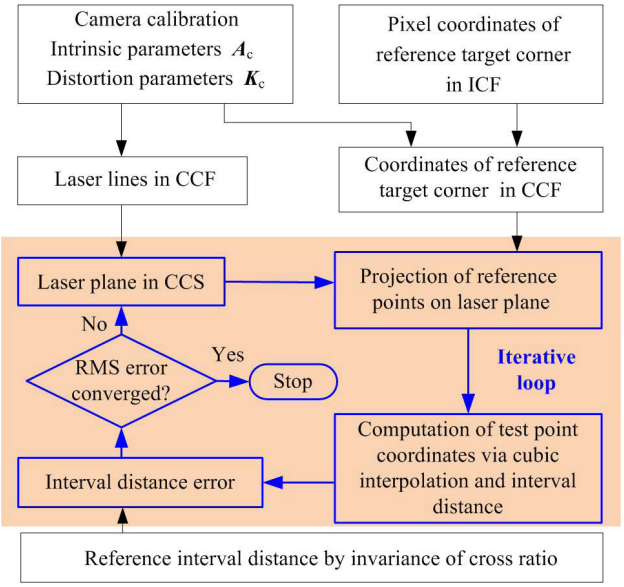

FIGURE 3. Calibration procedures.

III. SENSOR CALIBRATION

A. CAMERA MODEL

Assuming P has a homogeneous world coordinates of $(X, Y, Z, 1)$, its camera coordinates can be computed by

$$[x_c y_c z_c 1]^T = \boldsymbol{H}_c^w [X \;\; Y \;\; Z \;\; 1]^T \tag{1}$$

where $\boldsymbol{H}_c^w$ is the coordinate transformation matrix from WCF to CCF. The normalized projection coordinates of P on Π_I are

$$[x, y]^T = [x_c/z_c, y_c/z_c]^T \tag{2}$$

The projection coordinates after taken into account of the radial and tangential distortions are

$$\begin{cases} x' = x(1 + k_1 r^2 + k_2 r^4) + 2p_1 xy + p_2(r^2 + 2x^2) \\ y' = y(1 + k_1 r^2 + k_2 r^4) + p_1(r^2 + 2y^2) + 2p_2 xy \end{cases} \tag{3}$$

where $\boldsymbol{K}_c = [k_1, k_2, p_1, p_2]$ are the distortion parameters, and $r^2 = x^2 + y^2$. The image coordinates can then be computed by

$$\begin{bmatrix} u \\ v \\ 1 \end{bmatrix} = \boldsymbol{A}_c \begin{bmatrix} x' \\ y' \\ 1 \end{bmatrix}, \quad \boldsymbol{A}_c = \begin{bmatrix} f_x & 0 & u_0 \\ 0 & f_y & v_0 \\ 0 & 0 & 1 \end{bmatrix} \tag{4}$$

where $\boldsymbol{A}_c$ is the intrinsic parameter matrix, f_x and f_y are the focal length, u_0 and v_0 are image coordinates of the principal point.

B. CALCULATE INITIAL LASER PLANE

The initial laser plane is achieved by fitting of the laser lines in CCF. The camera coordinate of the points on each laser line is achieved by use of a dot target. A local coordinate

system (LCS) is established on the target with its Z axis perpendicular to the target plane, the local coordinates for each dot center can be obtained from the target parameters. If the intrinsic matrix $\boldsymbol{A}_{\mathrm{c}}$ and distortion parameters $\boldsymbol{K}_{\mathrm{c}}$ are known, the extrinsic matrix for the nth placement of the target can be achieved by Tsai's method [37], as

$$\mathbf{H}_{c,n}^{L} = \begin{bmatrix} r_{1,n} & r_{2,n} & r_{3,n} & T_{x,n} \\ r_{4,n} & r_{5,n} & r_{6,n} & T_{y,n} \\ r_{7,n} & r_{8,n} & r_{9,n} & T_{z,n} \\ 0 & 0 & 0 & 1 \end{bmatrix} \tag{5}$$

where $r_{i,n}$, $i = 1, 2, \ldots, 9$, are rotation parameters, $T_{x,n}$, $T_{y,n}$ and $T_{z,n}$ are translation values. For an arbitrary point with the local coordinates of (X^L, Y^L, Z^L), its camera coordinates can be computed by

$$[x_c\ y_c\ z_c\ 1]^{\mathrm{T}} = \boldsymbol{H}_{c,n}^{L} \begin{bmatrix} X^L & Y^L & Z^L & 1 \end{bmatrix}^{\mathrm{T}} \tag{6}$$

For the stripe lays on the target, Z^L coordinate of arbitrary stripe center point is 0. The normalized camera coordinates of $C(u, v)$ with distortion is

$$\begin{bmatrix} x', y', 1 \end{bmatrix}^T = \boldsymbol{A}_c^{-1} \cdot [u, v, 1]^T \tag{7}$$

The ideal projection coordinates (x, y) can be achieved by solving the distortion Eq. (3) via Newton iteration. The X^L and Y^L coordinates in LCS can be calculated by

$$\begin{bmatrix} X^L \\ Y^L \end{bmatrix} = \begin{bmatrix} r_{1,n} - x \cdot r_{7,n} & r_{2,n} - x \cdot r_{8,n} \\ r_{4,n} - y \cdot r_{7,n} & r_{5,n} - y \cdot r_{8,n} \end{bmatrix}^{-1} \cdot \begin{bmatrix} x \cdot T_{z,n} - T_{x,n} \\ y \cdot T_{z,n} - T_{y,n} \end{bmatrix} \tag{8}$$

Thus, for any stripe center point, its coordinates in LCS can be obtained. By substituting these coordinates into Eq. (6), their camera coordinates can be obtained. For one target placement, one laser line in CCS is achieved. By fitting all the laser lines, the initial laser plane can be obtained and denoted by

$$B_1^{(0)} x_{\mathrm{c}} + B_2^{(0)} y_{\mathrm{c}} + B_3^{(0)} z_{\mathrm{c}} + B_4^{(0)} = 0 \tag{9}$$

where, $B_1^{(0)}, B_2^{(0)}, \ldots, B_4^{(0)}$ are the initial coefficients.

C. CALCULATE WORLD COORDINATES

In CCF, the equation of each projection line that passes though the kth reference point $P_k^T(x_k^T, y_k^T, z_k^T)$ can be expressed by

$$\frac{x_c}{x_k^{\mathrm{T}}} = \frac{y_c}{y_k^{\mathrm{T}}} = \frac{z_c}{z_k^{\mathrm{T}}} \tag{10}$$

By combining Eq. (9) and (10), coordinates of projection points P_k^L can be obtained. Thus, for each corner point that has known pixel coordinates, its corresponding points on Π_{L} have been obtained. In WCF, the Z coordinate of each projection point is 0, and the X and Y coordinates can be obtained by calculating the distance to $O_{\mathrm{w}}Y_{\mathrm{w}}$ and $O_{\mathrm{w}}X_{\mathrm{w}}$ axes, respectively. Then two surfaces, named S_x and S_y, are generated by cubic interpolation. They describe the homographic mapping relationship from the image coordinates (u, v) to X_{w} and Y_{w}, respectively.

D. DATA-DRIVEN LASER PLANE OPTIMIZATION

The laser lines in CCF, which are used for fitting of Π_{L}, rely on the extrinsic and the intrinsic parameters of the camera. To refine Π_{L}, the interval distances between test points are first calculated based on the invariance of cross ratio as shown by Fig. 4, where $D_{1,m}, D_{2,m}, D_{3,m}$ are collinear points (center points) of the mth column on target and $C_{1,m}$, $C_{2,m}$, $C_{3,m}$ are their corresponding image points. $C_{4,m}$ is the intersection point between the fitted line and the laser line, and $D_{4,m}$ is the test point of $C_{4,m}$.

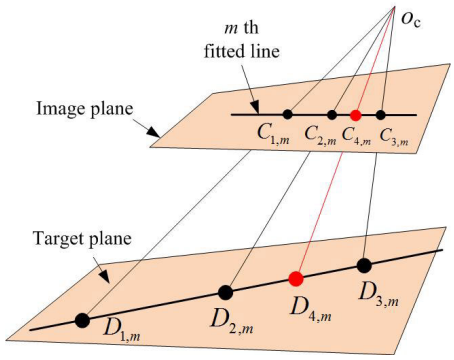

FIGURE 4. World coordinates calculation via the invariance of cross-ratio.

The cross ratio value for the four points on image plane can be expressed as

$$\lambda_m = CR(C_{1,m}, C_{2,m}; C_{3,m}, C_{4,m}) = \frac{C_{1,m}C_{3,m}/C_{2,m}C_{3,m}}{C_{1,m}C_{4,m}/C_{2,m}C_{4,m}} \tag{11}$$

Based on the invariance of cross ratio, the actual distance of $|D_{2,m}D_{4,\,m}|$ satisfies Eq. (12)

$$\lambda_m = \frac{|D_{1,m}D_{3,m}| \,/\, |D_{2,m}D_{3,m}|}{|D_{1,m}D_{4,m}| \,/\, |D_{2,m}D_{4,m}|} = \frac{2\,|D_{2,m}D_{4,m}|}{I_d + |D_{2,m}D_{4,m}|} \tag{12}$$

where I_d is the ideal distance of target point intervals. By solving Eq. (12), the value of $|D_{2,m}D_{4,m}|$ can be obtained. For the $(m+1)$th column, the value of $|D_{2,m+1}D_{4,m+1}|$ can be computed similarly. It can be seen that $D_{2,m}D_{4,m}D_{4,m+1}D_{2,m+1}$ constitute a right-angled trapezoid. Thus, the reference distance I_m^R of $|D_{4,m}D_{4,m+1}|$ can be expressed by

$$I_m^R = \sqrt{I_d^2 + \left(|D_{2,m}D_{4,m}| - |D_{2,m+1}D_{4,m+1}|\right)^2} \tag{13}$$

World coordinates of the intersection points can also be computed by use of the mapping surfaces with the interval distance between the mth and $(m+1)$th intersection points denoted by I_m^W. The error of the interval distance can be calculated by

$$E_m^I = I_m^{\mathrm{W}} - I_m^R \tag{14}$$

The mapping surfaces rely on Π_{L} directly. The values of E_m^I will change accordingly with the position of Π_{L}. To find

the best plane equation, the calibration target is placed within the measurement field of view (FOV) at Q different positions. For each position, $M-1$ distance errors can be obtained, where M is the column number of target points. Taken into account the data set of all interval distance errors, the optimization model can be expressed by

$$E_{\text{rms}} = \sqrt{\frac{1}{Q(M-1)}\sum_{q=1}^{Q}\sum_{m=1}^{M-1}\left[I^{\text{W}}_{m,q}(B^{(k)}_1, B^{(k)}_2, B^{(k)}_3, B^{(k)}_4) - I^{\text{R}}_{m,q}\right]^2} \tag{15}$$

where $B^{(k)}_1, B^{(k)}_2, \ldots, B^{(k)}_4$ are the coefficients of Π_{L} for the kth iteration, $I^{\text{W}}_{m,q}$ and $I^{\text{R}}_{m,q}$ are the mth interval distance for the qth target placement. The optimization model is then solved by the sequential quadratic programming (SQP) method [38].

IV. SENSOR CALIBRATION AND ANALYSIS

A. CAMERA MODEL

The measurement system with LSLS is shown by Fig. 5. The laser line projector (Guangdong Shenzuan Lasers co., Ltd) has the wavelength of 650nm and the power of 5mW. Its minimum line width can reach 0.3mm at the projection distance of 300mm. The camera (MV-UB500M, Shenzhen Mindvision Technology co., Ltd) has a resolution of 2592 × 1944 pixels with a 4∼12mm variable focal lens. The checkerboard target (CC-100) and the dot target (HC-60) are both from Shenzhen PointVision technology co., Ltd. The position accuracy of the targets is better than 1μm. The checkerboard target has the square array of 15 × 19 with the side length of 5mm. It is used for the camera calibration and taken as the reference target. The dot target has 9 × 9 dots array with an interval of 6mm. It is used for initial laser plane computation and accuracy verification.

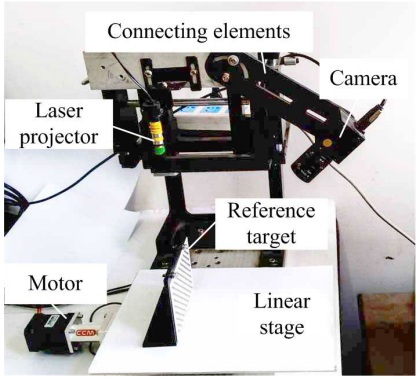

FIGURE 5. Configuration of the system.

B. CALIBRATION PROCEDURES

The reference target is mounted on an L-shaped supporter with its marker surface perpendicular with the linear stage. Relative position of the laser projector and the target is manually adjusted to generally align the marker surface with Π_{L}. After that, the lens is also adjusted to make the target image as clear as possible, and fulfill the camera's FOV. To guarantee the image quality, the laser projector is turned off at this instance. The reference target image with extracted corner points is shown by Fig. 6. The area that covered by the corner points also denotes the measuring range. It can be computed from the target parameters and is 75mm×95mm. Then, the target is freely placed to other 11 different positions to get the corresponding images. Together with the reference target image, twelve images are now obtained for camera calibration via the software package developed by Bouguet [39].

The intrinsic matrix and the distortion parameters are

$$\boldsymbol{A}_{\text{c}} = \begin{bmatrix} 5490.81 & 0 & 1341.51 \\ 0 & 5488.61 & 878.21 \\ 0 & 0 & 1 \end{bmatrix} \tag{16}$$

$$\boldsymbol{K}_{\text{c}} = \begin{bmatrix} -0.04857 & 0.23257 & 0.00037 & 0.0007 \end{bmatrix} \tag{17}$$

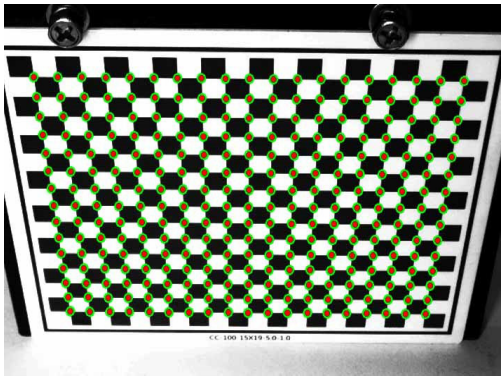

FIGURE 6. Image of reference target and corner points.

The average re-projection errors in u and v directions are 0.1143 pixel and 0.1172 pixel, respectively. This indicates high camera calibration accuracy. By use of the software package, the extrinsic parameters of the reference target can also be obtained, and the coordinate of reference points can be computed in CCF.

The laser plane is computed by use of the dot target. The target is placed within the camera's FOV and intersects with Π_{L}. Then, the laser projector is turned off to get a clear target image. The dot centers are achieved via the ellipse fitting of dot edges. For the actual interval distance of the dots and the camera parameters are known, the corresponding extrinsic matrix for this placement of the target $H^{L}_{c,n}$ can be obtained by use of Tsai's method [37]. Keep the position of the target unchanged, turn on the laser projector and adjust the expose time to get a high quality laser stripe. The center points of the stripe is extracted by use of the improve gray-gravity method [40]. The center points are also plotted on the image of the target as shown by Fig. 7(a). The intersection points between the stripe line and the fitted line of each column dot centers can be computed. Their corresponding points, also called the test points, can be obtained using the method in section 3.2, as shown by Fig. 7(b).

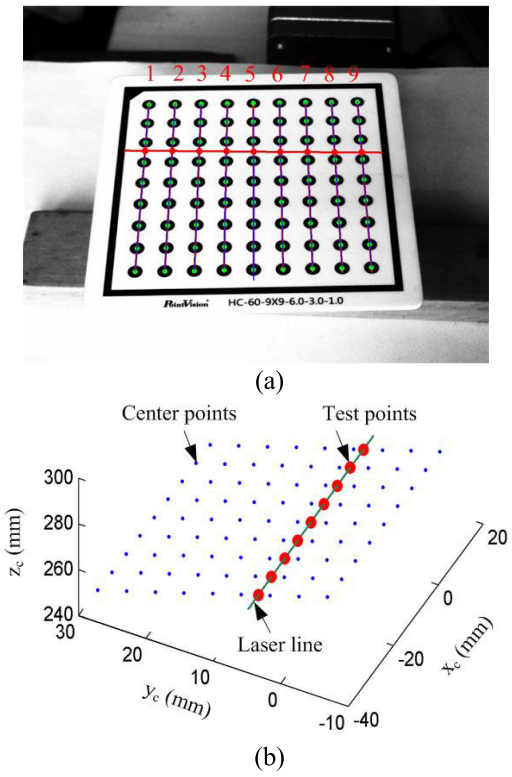

FIGURE 7. Computation of laser line in CCF, (a) Image of dot target, (b) computed laser line.

The position of dot target is changed within the camera's FOV. One laser line can be obtained for a specific position. In this experiment, the target was placed at 12 different positions and 12 laser lines can be obtained in CCF. By fitting these lines, the initial laser plane can be obtained as

$$0.0053x_c - 0.7294y_c + 0.6841z_c + 180.7711 = 0 \quad (18)$$

The projection lines are determined by the reference points and the origin of the CCF. The projection points are the intersection points between the projection lines and the laser plane, as shown by Fig. 8. The world coordinates for each projection point can be computed by use of the method in section 3.3. For each projection point has the same image coordinate with the reference point, two mapping surfaces, $S_x(u, v, X_w)$ and $S_y(u, v, Y_w)$, can be established, as shown by Fig. 9 (a) and (b). Each surface is represented by discrete points. Thus, the X_w and Y_w coordinates of an arbitrary point within the measurement scope can be computed via cubic interpolation of S_x and S_y, respectively.

To evaluate the accuracy, the interval distances between the test points are calculated from the mapping surfaces and their reference distances are obtained based on the invariance of cross ratio. The position of the test points on laser plane is shown by Fig. 10. These points generally cover the measuring range of the senor, so the evaluation result is credible.

For each target placement, eight interval distances can be obtained. The target is moved to 12 different positions successively, and 96 interval distances can be got. The coefficients

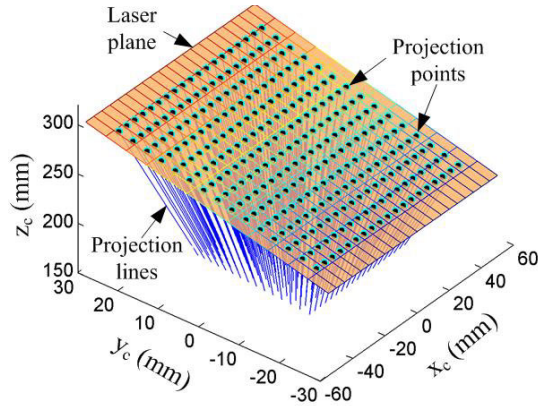

FIGURE 8. Calculating the projection points on laser plane.

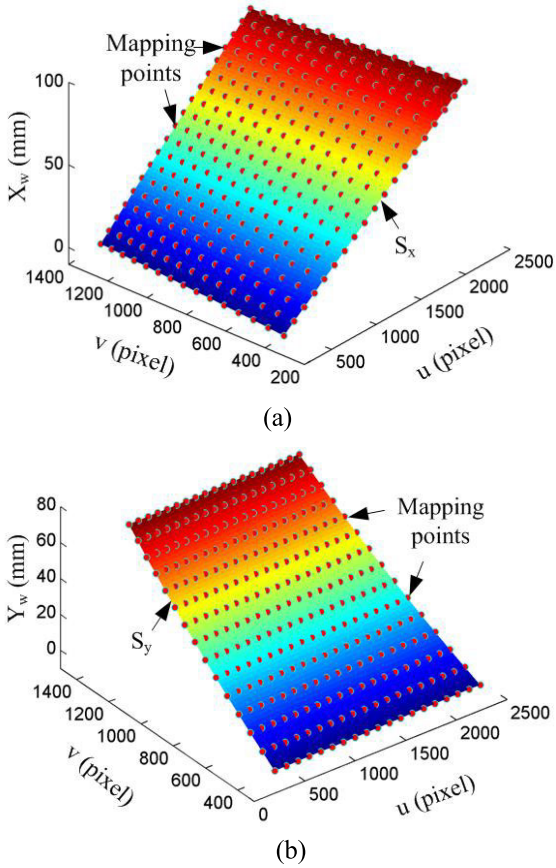

FIGURE 9. Coordinates mapping surfaces, (a) S_x for X_w calculation, (b) S_y for Y_w calculation.

of the laser plane are optimized and the convergence curve can be shown by Test 1 in Fig. 11. The laser plane equation after optimization is

$$0.0003x_c - 0.7231y_c + 0.6835z_c + 180.7713 = 0 \quad (19)$$

For Test 1, the E_{rms} value can be reduced from 0.019mm to 0.003mm via the optimization. This also denotes a significant improvement of the calibration accuracy. To validate the robustness, two and four laser lines are randomly removed for the fitting of initial laser plane. Their corresponding

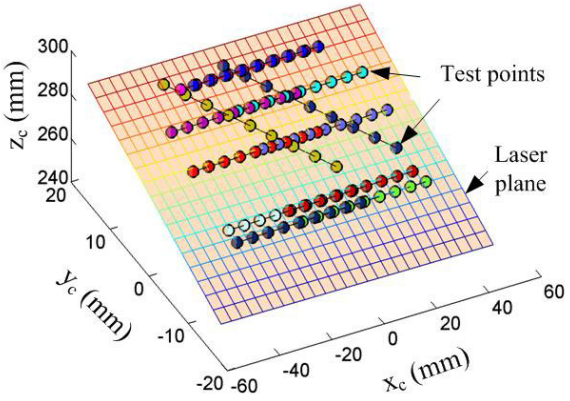

FIGURE 10. Test points for distance evaluation.

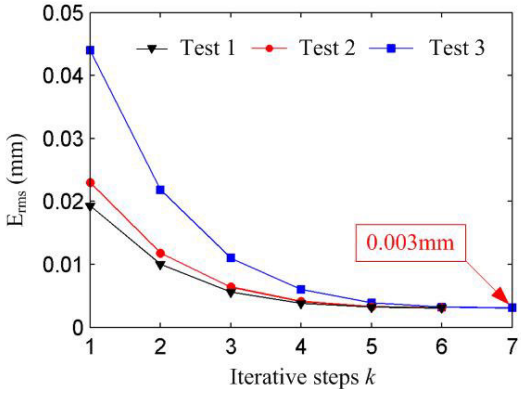

FIGURE 11. Convergence curve for optimization.

convergence curves are shown by Test 2 and Test 3, respectively. It can be seen that though the initial E_{rms} values get larger with fewer laser lines, all of them can converge to the same value of 0.003mm within 7 iteration steps. Therefore, the final laser plane would not rely on the models in Section 3.2 anymore.

Fig. 12(a) is the interval distance error before and after optimization with a maximum value of just 0.009mm. The accumulated distance is the distance between the current and the first test point. To further validate the proposed method, the accumulated distance error E_m^A can be defined as

$$E_m^A = \left|D_{4,m+1}D_{4,1}\right| - I_m^A \tag{20}$$

where $|D_{4,m+1}D_{4,1}|$ is the accumulated distance from the $(m+1)$th test point to the first one with $m = 1, 2, \ldots, 8$, and I_m^A is the reference distance calculated by the invariance of cross ratio. The error values are shown by Fig. 12(b) with the RMS value of E_m^A reduced from 0.047mm to 0.005mm though the optimization process.

V. DISCUSSIONS

A. REFINE PIXEL COORDINATES OF REFERENCE POINTS

From the numerical calibration process, it can be seen that the corner extraction error of reference points would influence the measurement result directly. The pixel coordinates of each corner is extracted individually with an independent error

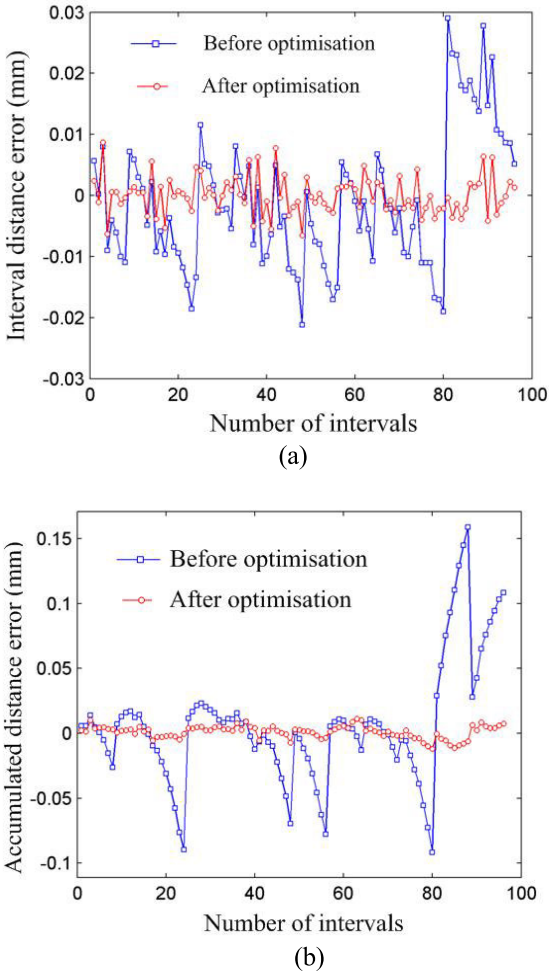

FIGURE 12. Distance errors before and after optimization, (a) interval errors, (b) accumulated errors.

distribution. To get a better result, all the corner points are projected onto the normalized image plane to remove the distortion effects. Then, they are fitted in lines and columns as shown by Fig. 13. The intersection points are considered the ideal points on the normalized image plane. By re-projecting them onto the image plane, the image coordinate of new corner points can be obtained. These refined points are taken as the ideal pixel points for constructing the triangle patches.

To evaluate the re-projection on the measurement results, the interval distances are also computed the same as section 4.2. The interval distance error is shown by Fig. 14, where E_{before} and E_{after} are the interval distance errors before and after the corner coordinate refinement, respectively. It can be seen that E_{after} has a smaller fluctuation. The RMS values of E_{before} and E_{after} are 0.006mm and 0.004mm, and their maximum deviations are 0.011mm and 0.006mm, respectively. So the refined pixel coordinates can reduce the measurement error and improve the measurement accuracy to some extent.

B. COMPARISON ANALYSIS

To show the accuracy of the numerical method, it is compared with the classical model based method proposed by

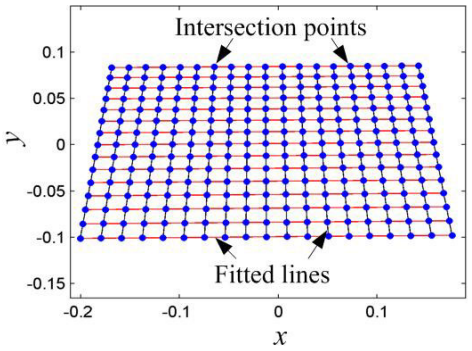

FIGURE 13. Recalculate corner projection points on normalized image plane.

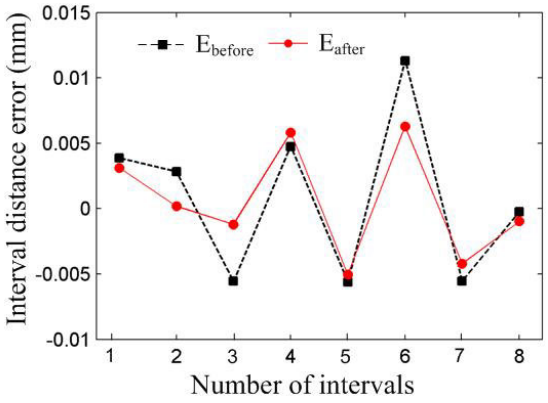

FIGURE 14. Affection of reference pixel points coordinate refinement on the measured result.

Zhou and Zhang [9]. Here, only the accumulated distances between the test point pairs are calculated by use of Zhou's method [9] and our method, respectively. The test points are from the first position of the dot target, shown in Fig.7(a). Their reference distances are calculated based on the invariance of the cross ratio. The results are shown in Table 1. It can be seen that the proposed method can achieve a higher accuracy with the same hardware setup.

Similarly as the above error analysis process, the distance errors of each point pair for the left 11 positions of the target are all calculated by use of Zhou's method and the proposed method. The statistical results are shown in Table 2. The RMS value can reach 0.005mm which is reduced by 91.5% compared with that of Zhou's method. The maximum deviation (MD) and the average (AVR) values are also reduced more than 90%. Therefore, the proposed method can significantly improve the calibration accuracy via the numerical mapping and the data-driven laser plane optimization strategies.

C. MEASUREMENT OF STEPS

Four bilateral steps are designed and milled on a precision milling machine for accuracy evaluation, as shown by Fig. 15(a). The upper step is taken as the reference plane and the rest steps are named as S_1, S_2 and S_3. Their corresponding

TABLE 1. Comparison of the measuring results with the classical method (Unit: mm).

Point pairs	Reference distances	Zhou's Method [9]		Proposed method	
		Calculated distance	Error	Calculated distance	Error
(1, 2)	6.001	6.002	0.001	6.004	0.003
(1, 3)	12.002	12.001	-0.001	12.004	0.002
(1, 4)	18.003	18.002	-0.001	18.013	0.010
(1, 5)	24.004	23.993	-0.011	24.008	0.004
(1, 6)	30.005	29.985	-0.020	30.010	0.005
(1, 7)	36.006	35.971	-0.035	36.011	0.005
(1, 8)	42.007	41.951	-0.056	42.011	0.004
(1, 9)	48.008	47.927	-0.081	48.011	0.003

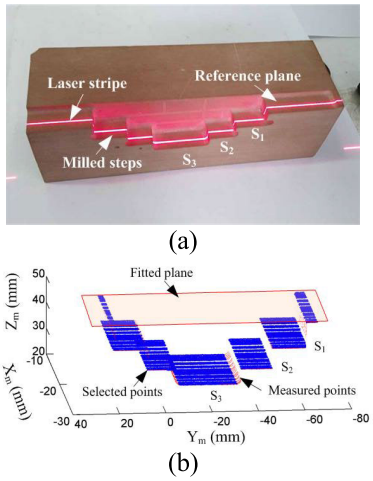

FIGURE 15. Measurement of steps, (a) photo of steps, (b) measurement results.

TABLE 2. Error analysis of the measuring results (Unit: mm).

	MD	AVR	RMS
Zhou's method [9]	-0.170	0.044	0.059
Proposed method	-0.012	0.004	0.005
Reduced by	92.9%	90.9%	91.5%

heights are denoted by h_1, h_2 and h_3. The steps are scanned on the measurement system with the results shown by Fig. 15(b).

For accuracy evaluation, the boundary points that are not on the planar steps are excluded. The reference plane is firstly calculated by plane fitting. Then, the average distance to the reference plane is computed for each step. Also taken the upper step as the reference, the height of other steps is measured on the coordinate measuring machine (Hexagon Golbal 7107). The measurement results and the errors are shown in Table 3. The height error for h3 is -0.007mm with the relative error of -0.03%. No accumulated error can be observed from the results. This further validates the high accuracy of the proposed method.

D. ERROR ANALYSIS

To clarify the merits of our method, the factors that contribute to the final calibration error are analyzed, as shown by Fig. 16.

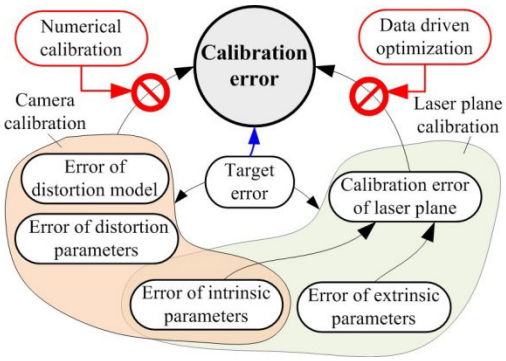

FIGURE 16. Error analysis of the calibration method.

TABLE 3. Error analysis of the measuring results (Unit: mm).

No.	CMM	LSLS	Error	Relative error
h_1	10.002	9.995	-0.007	-0.07%
h_2	18.003	17.997	-0.006	-0.03%
h_3	24.004	23.997	-0.007	-0.03%

For the model based methods [6]–[24], the calibration error generally comes from two parts. One is the camera calibration including the determination of distortion models, the calibration of distortion and intrinsic parameters. The other is the laser plane calibration which also relies on intrinsic parameters and the extrinsic parameters of each target placement. These two parts constitute the complete solution of the sensor model [9]. Meanwhile, all the errors denoted in the two parts would contribute to the calibration error directly. Therefore, the accuracy of the traditional method that relies on these models of the two parts has become rather difficult to be improved.

Our method, on the other hand, can cut off the undesired effects of the above errors on the final calibration result. By projecting the target corner points onto the laser plane, we established the numerical mapping relationship between the projection points and their pixel coordinates. This numerical model does not rely on the camera models anymore. The data-driven laser plane optimization is based on the interval error data that obtained by use of the invariance of cross ratio which does not rely on camera model nether. Moreover, the test points that are selected for the accuracy evaluation are from 12 individual intersection lines. They can well represent the laser plane and provide reasonable data for the optimization. The optimization that takes into account all the error values can come to a global optimization solution. Thus, only the target error (e.g. target fabrication error, corner extraction error) plays a dominate role on the calibration accuracy.

Though high calibration results can be reached, the proposed calibration method also has its shortcomings. One is the measurement range is restricted by the reference target, so it is not suited for the sensors that are used for measuring large parts. Another is the method has more calibration steps than the traditional methods. Not only the camera intrinsic parameters and the initial coefficients of the laser plane need to be calibrated, but also the additional optimization process is required to refine the laser plane. Despite this, the complicated calibration process rewards extremely high calibration results.

VI. CONCLUSION

A high precision numerical calibration method is proposed for the LSLS which also involves a data-driven laser plane optimization procedure. To establish the numerical mapping relationship between the pixel coordinates and the world coordinates, the laser plane is firstly calculated by used of the calibrated camera parameters, and then optimized based on the RMS value of the interval distance error. The reference interval distance is computed by use of the invariance of the cross-ratio. Thus, it is not affected by the camera and the laser plane model. Through the optimization process, the coefficients of the laser plane can be fine adjusted. By projecting the reference points onto the laser plane, the final homographic relationship, which no more relies on the camera model, can be established. The unfavorable influence of the model introduced errors can be basically eliminated. The RMS value of the calibration error can reach 0.005mm, significantly improved than the traditional method. The measurement of the steps further validates the proposed calibration method.

REFERENCES

[1] G. Sansoni, M. Trebeschi, and F. Docchio, "State-of-the-art and applications of 3D imaging sensors in industry, cultural heritage, medicine, and criminal investigation," *Sensors*, vol. 9, no. 1, pp. 568–601, Jan. 2009.
[2] Y. Yang, L. Liu, B. Yi, and F. Chen, "An accurate and fast method to inspect rail wear based on revised global registration," *IEEE Access*, vol. 6, pp. 57267–57278, 2018.
[3] Y. Li, J. Zhou, Q. Mao, J. Jin, and F. Huang, "Line structured light 3D sensing with synchronous color mapping," *IEEE Sensors J.*, vol. 20, no. 17, pp. 9796–9805, Sep. 2020.
[4] M. Rahayem, N. Werghi, and J. Kjellander, "Best ellipse and cylinder parameters estimation from laser profile scan sections," *Opt. Lasers Eng.*, vol. 50, no. 9, pp. 1242–1259, Sep. 2012.
[5] X. Lu, D. Gu, Y. Wang, Y. Qu, C. Qin, and F. Huang, "Feature extraction of welding seam image based on laser vision," *IEEE Sensors J.*, vol. 18, no. 11, pp. 4715–4724, Jun. 2018.
[6] R. Dewar, "Self-generated targets for spatial calibration of structured-light optical sectioning sensors with respect to an external coordinate system," in *Proc. Robots Vis. Conf.*, 1988, pp. 5–13.
[7] F. Duan, F. Liu, and S. H. Ye, "A new accurate method for the calibration of line structured light sensor," *Chin. J. Sci. Instrum.*, vol. 1, pp. 108–110, Oct. 2000.
[8] D. Huynh, R. Owens, and P. Hartmann, "Calibrating a structured light stripe system: A novel approach," *Int. Jour. Comput. Vis.*, vol. 33, pp. 73–86, Sep. 1999.
[9] F. Zhou and G. Zhang, "Complete calibration of a structured light stripe vision sensor through planar target of unknown orientations," *Image Vis. Comput.*, vol. 23, no. 1, pp. 59–67, Jan. 2005.
[10] Z. Wei, "Calibration approach for structured-lighted-stripe vision sensor," *Chin. J. Mech. Eng.*, vol. 41, no. 2, p. 210, 2005.
[11] Z. Zhang, "A flexible new technique for camera calibration," *IEEE Trans. Pattern Anal. Mach. Intell.*, vol. 22, no. 11, pp. 1330–1334, 2000.
[12] Z. Qiu and J. Xiao, "New calibration method of line structured light vision system and application for vibration measurement and control," *Opt. Precis. Eng.*, vol. 27, no. 1, pp. 230–240, 2019.
[13] M. Lu, W. Ge, A. Zhou, G. Lv, and F. Zhou, "Calibrating laser scanning probe with double virtual circle target," *Acta. Opt. Sin.*, vol. 34, no. 10, pp. 205–211, 2014.

[14] G. Xu, L. Sun, X. Li, J. Su, Z. Hao, and X. Lu, "Global calibration and equation reconstruction methods of a three dimensional curve generated from a laser plane in vision measurement," *Opt. Exp.*, vol. 22, no. 18, pp. 22043–22055, Sep. 2014.
[15] T. Chen, J. Zhao, and X. Wu, "New calibration method for line structured light sensor based on planar target," *Acta. Opt. Sin.*, vol. 35, no. 1, pp. 180–188, 2015.
[16] M. Shao, J. Dong, and A. Hirpa Madessa, "A new calibration method for line-structured light vision sensors based on concentric circle feature," *J. Eur. Opt. Soc.-Rapid*, vol. 15, no. 1, pp. 1–11, Dec. 2019.
[17] Z. Liu, X. Li, F. Li, and G. Zhang, "Calibration method for line-structured light vision sensor based on a single ball target," *Opt. Lasers Eng.*, vol. 69, pp. 20–28, Jun. 2015.
[18] P. Zhou, K. Xu, and D. Wang, "Rail profile measurement based on line-structured light vision," *IEEE Access*, vol. 6, pp. 16423–16431, 2018.
[19] W. Zou, Z. Wei, and F. Liu, "High-accuracy calibration of line-structured light vision sensors using a plane mirror," *Opt. Exp.*, vol. 27, no. 24, pp. 34681–34704, Nov. 25 2019.
[20] J. Santolaria, J. J. Pastor, F. J. Brosed, and J. J. Aguilar, "A one-step intrinsic and extrinsic calibration method for laser line scanner operation in coordinate measuring machines," *Meas. Sci. Technol.*, vol. 20, no. 4, Apr. 2009, Art. no. 045107.
[21] Z. Xie and A. Zhang, "Simultaneous calibration of the intrinsic and extrinsic parameters of ultra-large-scale line structured-light sensor," *Acta. Opt. Sin.*, vol. 38, no. 3, pp. 322–330, 2018.
[22] J. Zhou, Y. Li, Z. Qin, F. Huang, and Z. Wu, "Calibration of line structured light sensor based on reference target," *Acta. Opt. Sin.*, vol. 39, no. 4, pp. 169–176, 2019.
[23] X. Pan and Z. Liu, "High-accuracy calibration of line-structured light vision sensor by correction of image deviation," *Opt Exp.*, vol. 27, no. 4, pp. 4364–4385, Feb. 18 2019.
[24] X. Pan, Z. Liu, and G. Zhang, "High-accuracy calibration of on-site multi-vision sensors based on flexible and optimal 3D field," *IEEE Access*, vol. 7, pp. 159495–159506, 2019.
[25] N. Van Gestel, S. Cuypers, P. Bleys, and J.-P. Kruth, "A performance evaluation test for laser line scanners on CMMs," *Opt. Lasers Eng.*, vol. 47, nos. 3–4, pp. 336–342, Mar. 2009.
[26] X. Zhang and J. Zhang, "Summary on calibration method of line-structured light sensor," in *Proc. IEEE Int. Conf. Robot. Biomimetics (ROBIO)*, Dec. 2017, pp. 1142–1147.
[27] Z. Xie, X. Wang, and S. Chi, "Simultaneous calibration of the intrinsic and extrinsic parameters of structured-light sensors," *Opt. Lasers Eng.*, vol. 58, pp. 9–18, Jul. 2014.
[28] L. Ma, Y. Chen, and K. L. Moore, "Rational radial distortion models of camera lenses with analytical solution for distortion correction," *Int. J. Inf. Acquisition*, vol. 01, no. 02, pp. 135–147, Jun. 2004.
[29] L. Deng, G. Lu, Y. Shao, M. Fei, and H. Hu, "A novel camera calibration technique based on differential evolution particle swarm optimization algorithm," *Neurocomputing*, vol. 174, pp. 456–465, Jan. 2016.
[30] Z. Zhu and S. Li, "Lens distortion and proofreading technology," *Opt. Techn.*, vol. 31, pp. 136–138, Dec. 2005.
[31] J. Wang, F. Shi, J. Zhang, and Y. Liu, "A new calibration model of camera lens distortion," *Pattern Recognit.*, vol. 41, no. 2, pp. 607–615, Feb. 2008.
[32] W. Li, S. Shan, and H. Liu, "High-precision method of binocular camera calibration with a distortion model," *Appl. Opt.*, vol. 56, no. 8, pp. 2368–2377, 2017.
[33] S. Yang, X. Shi, G. Zhang, and C. Lv, "A dual-platform laser scanner for 3D reconstruction of dental pieces," *Engineering*, vol. 4, no. 6, pp. 796–805, Dec. 2018.
[34] Q. Wu, T. He, and T. Shi, "A calibration method for line structured-light vision sensor based on a plane target," *J. Optoelectron., Laser*, vol. 24, no. 2, pp. 297–301, 2013.
[35] Y. Li, J. Zhou, and F. Huang, "High precision calibration of line structured light sensors based on linear transformation over triangular domain," *Proc. SPIE*, vol. 9684, Sep. 2016, Art. no. 968407.
[36] Y. Zou, M. Zhao, and L. Zhang, "Direct calibration method of laser stripe vision sensor based on gauge block," *Chin. J. Lasers*, vol. 41, no. 11, pp. 230–240, 2014.
[37] R. Tsai, "A versatile camera calibration technique for high-accuracy 3D machine vision metrology using off-the-shelf TV cameras and lenses," *IEEE J. Robot. Autom.*, vol. 3, no. 4, pp. 323–344, Aug. 1987.
[38] S. Yuwen, W. Xiaoming, G. Dongming, and L. Jian, "Machining localization and quality evaluation of parts with sculptured surfaces using SQP method," *Int. J. Adv. Manuf. Technol.*, vol. 42, nos. 11–12, pp. 1131–1139, Jun. 2009.
[39] J. Y. Bouguet. *The MATLAB Open Source Calibration Toolbox*. Accessed: Oct. 14, 2020. [Online]. Available: http://www.vision.caltech.edu/bouguetj/calib_doc/index.html
[40] Y. Li, J. Zhou, F. Huang, and L. Liu, "Sub-pixel extraction of laser stripe center using an improved gray-gravity method," *Sensors*, vol. 17, no. 4, pp. 814–827, 2017.

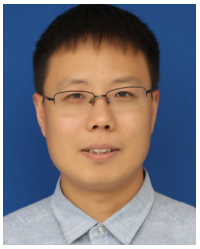

JINGBO ZHOU received the Ph.D. degree from the School of Mechanical Engineering, Harbin Institute of Technology, China, in 2013. He is currently an Associate Professor with the School of Mechanical Engineering, Hebei University of Science and Technology, Shijiazhuang, China. His research interests include milling of freeform surfaces and line structured light measurement.

LAISHENG PAN is currently pursuing the master's degree with the School of Mechanical Engineering, Hebei University of Science and Technology, Shijiazhuang, China. His current research interest includes line structured light sensors.

YUEHUA LI received the Ph.D. degree from the School of Mechanical Engineering, Harbin Institute of Technology, China, in 2013. She is currently an Associate Professor with the School of Mechanical Engineering, Hebei University of Science and Technology, Shijiazhuang, China. Her research interests include machine vision and optical sensing.

RENJIE DU is currently the General Manager with Hebei Boxline Intelligent Equipment Technology Company Ltd., Handan, China. His research interests include machine vision and automation.

FUXIANG ZHANG is currently a Professor with the School of Mechanical Engineering, Hebei University of Science and Technology, Shijiazhuang, China. His research interests include machine vision, optical sensing, and robotics.